

## Supplementary Information

### Dynamic Imaging of Nanostructures in an Electrolyte with a Scanning Electron Microscope

Aram Yoon<sup>1</sup>, Antonia Herzog<sup>1</sup>, Philipp Grosse<sup>1</sup>, Daan Hein Alsem<sup>2</sup>, See Wee Chee<sup>1\*</sup>, Beatriz Roldan Cuenya<sup>1</sup>

<sup>1</sup> Department of Interface Science, Fritz-Haber-Institute of the Max-Planck Society, Berlin, Germany

<sup>2</sup> Hummingbird Scientific, Lacey, WA, USA

\* Corresponding author: swchee@fhi-berlin.mpg.de

#### 1. Imaging condition in order to minimize the beam effect

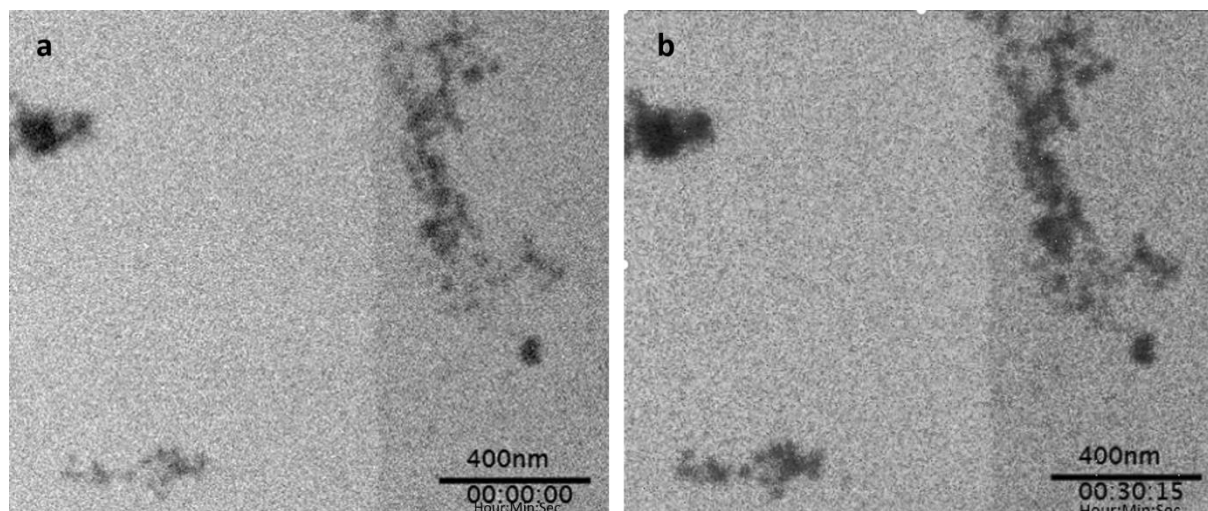


**Figure S1** Snapshots from Supplementary Movie 1 showing the  $\text{Cu}_2\text{O}$  NPs in 0.1 M  $\text{KHCO}_3$  at the start of imaging (a) and after 30 mins 15 s (b)

In our experiments, the imaging conditions were optimized by ensuring that there was not significant dissolution of the  $\text{Cu}_2\text{O}$  nanoparticles (NPs) during extended imaging (Lin *et al.* 2019)). For the frame rate used of 0.2 frames per second, the optimal probe current at 30 kV was found to be 25 pA. Figure S1 shows the results from such an experiment where we image the NPs more than 30 minutes of imaging. In this case, we observed instead a slight growth of the NPs, which we attribute it to a reaction between the NPs and the electrolyte. The provided supplementary video was accelerated by 200 times.

## 2. Resolution and signal to noise ratio

In our liquid cell SEM experiments, the image resolution is determined by the probe size and the signal-to-noise ratio. Figure S2 shows the simulated images (same as Figure 2c in main text) and the horizontal line profile across the Cu NPs. As the thickness increases, the noise level increases in both TE and BSE, and the difference between the minimum intensity and the maximum decreases. In the TE image with 500 nm water, the image contrast is the poorest as the image is in between bright and dark field. The numerical values of the signal-to-noise ratio (SNR) in the images confirms the observed trend with liquid thickness, which we quantify using the following metrics. Figure S3 shows the mean square error (MSE), the peak signal to noise ratio (PSNR), SNR and Weber contrast calculated by the following equation.

$$MSE = \frac{\sum_{M,N} [I_1(m,n) - I_{ref}(m,n)]^2}{M * N}$$

$$PSNR = 10 \log_{10} \left( \frac{1}{MSE} \right)$$

M and N are the number of the rows and columns in the image. The reference image is the binary image where the value at the particle is 1 and at the liquid area is zero. The SNR of the Cu and water are separately measured by the equation

$$SNR = \left( \frac{\mu}{\sigma} \right)^2$$

where  $\mu$  is the average signal value and  $\sigma$  is the standard deviation. Lastly, the Weber contrast is calculated by the following equation.

$$Contrast = \frac{\mu_{Cu} - \mu_{water}}{\mu_{water}}$$

where  $\mu_{Cu}$  and  $\mu_{water}$  are the average signal values at Cu and water respectively.

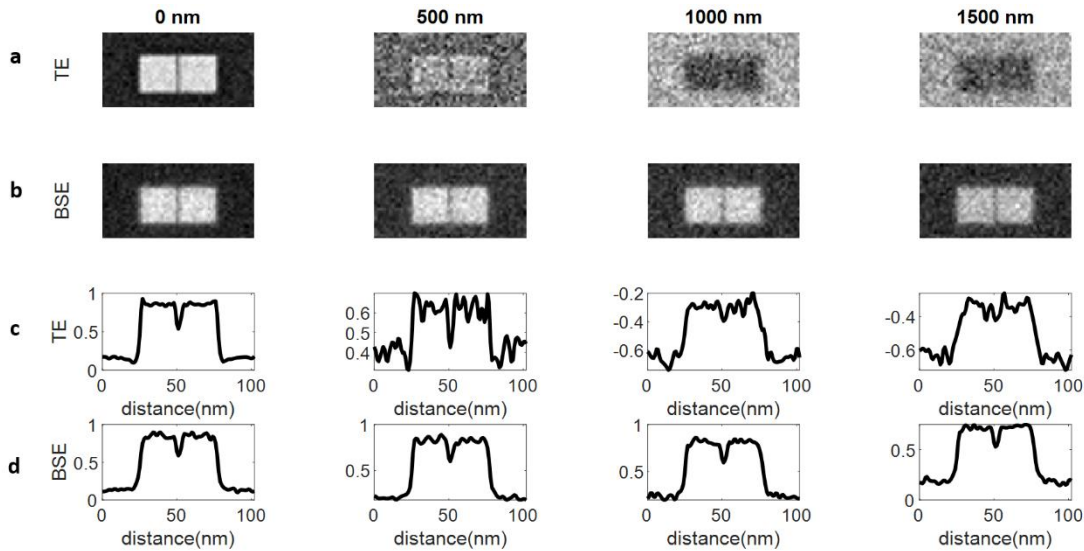


**Figure S2.** Image resolution as a function of the liquid thickness. (a) and (b) are the TE and BSE images respectively, with increasing liquid thickness from left to right. (c) and (d) indicate the horizontal line profile across two nanoparticles of TE and BSE images at each liquid thickness. The ADF angle is between 125-150 mrad.

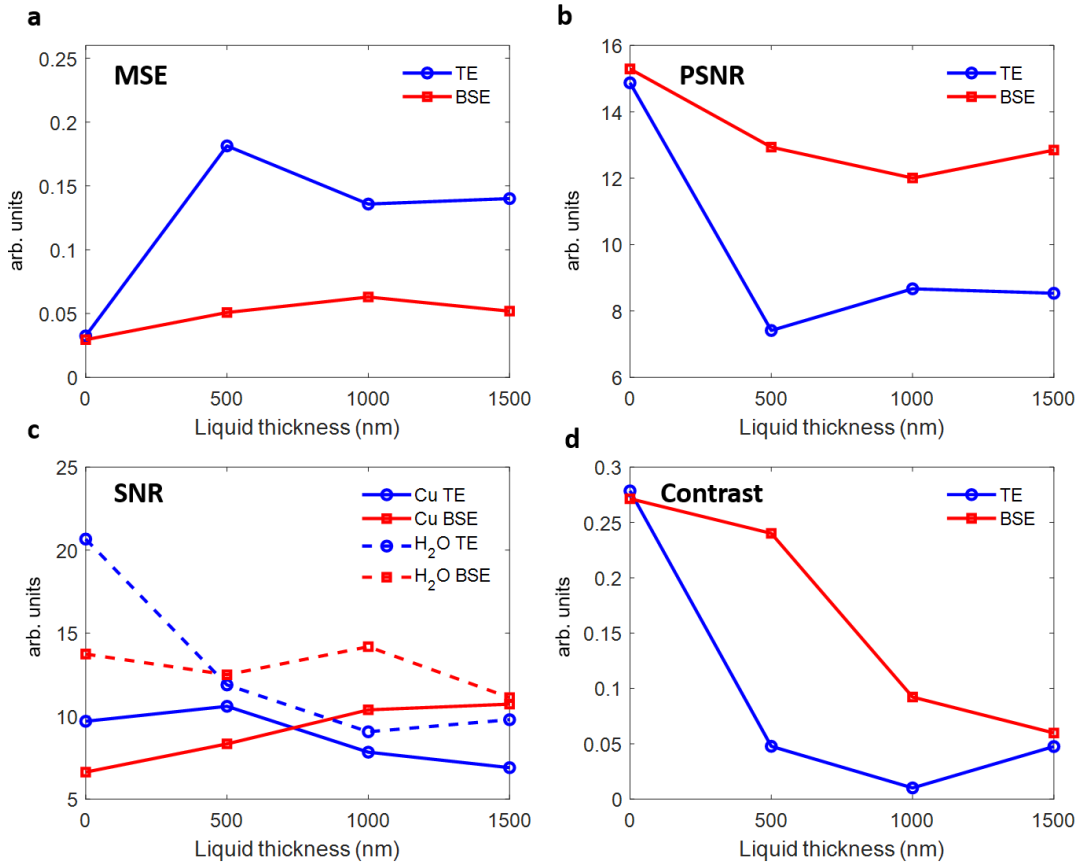


**Figure S3.** (a) MSE (b) PSNR, (c) SNR, and Weber contrast of TE and BSE images. The MSE increases and SNR decreases with the increasing thickness. The TE image at 500 nm particularly high MSE and low PSNR because it is at the angle where the BF to DF shift occurs and the intensity of water and Cu is almost identical.

Although the BSE signal does not lose its resolution, it suffers from a high noise level because only 0.002-0.3 % of the total intensity is transferred to BSE (Table 1). We mention here that the SNR and the contrast of the TE can be enhanced by integrating over a larger area of the annular dark field (ADF) detector.

### 3. Sharpness profile

The optimal position of the sample for liquid SEM is at the top membrane where the probe is only broadened by the top silicon nitride membrane and does not undergo further broadening in the liquid. The TE image will still be affected by the liquid thickness since TEs have to travel through the liquid after being scattered by the specimen. In Figure S4, we quantify the effect of liquid layer thickness on image resolution using the modular transfer function (MTF). The MTF is the Fourier transform of the line spread function and indicates how sharply we can resolve features. A broader MTF peak means that a sharp edge is resolved with less blurring. As shown in Figure S4(a) for TE and Figure S4(b) for BSE, the spatial resolution of TE is affected more significantly than that of BSE by the presence of the liquid. The MTF is translated to spatial resolution in Figure S4(c) where the resolution is defined as the frequency where MTF is equal to 0.1. The resolution of the TE image jumps from 1.25 to 3.7 nm when the liquid is thicker than 500 nm, whilst the resolution of BSE image is preserved below 1.5 nm.

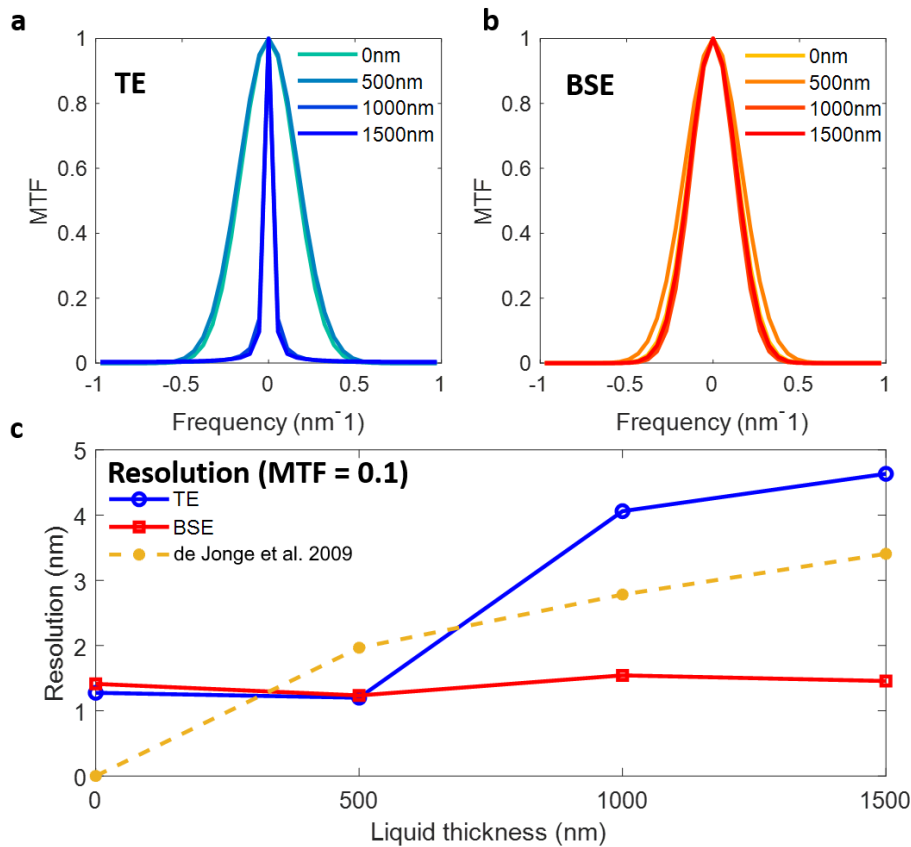


**Figure S4.** Sharpness analysis. (a) modular transfer function (MTF) of the TE image, (b) MTF of BSE image, (c) the nominal resolution of TE and BSE. The resolution is defined by the reciprocity of the frequency where the MTF is equal to 0.1. The theoretical resolution calculated using the model described in (de Jonge *et al.* 2009) is also included in (c).

The achievable resolution of objects in a liquid,  $d$ , can be calculated using the model described in (de Jonge *et al.* 2009)

$$d = 5l_{Cu} \sqrt{\frac{T}{N_0 l_{water}}}$$

where  $l_{Cu}$ , the inelastic mean free path, = 39 nm (estimated from NIST Electron Inelastic-Mean-Free Path Database by (C.J.Powell and Jablonski 2010)),  $l_{water}$ , the inelastic mean free path of

water, = 63 nm (LaVerne and Pimblott 1995) at 30 keV, and the number of the electrons used in the MC simulations of 78025 is designated as  $N_0$ , and  $T$  is the liquid layer thickness.

#### 4. Contrast Inversion

Figure S5 shows the simulated images of a Cu cube as a function of the liquid layer thickness and collection angle. The collection angle where the contrast goes from bright field to dark field shifts towards higher angles with increasing liquid thickness. Without liquid, the contrast transition occurs at 75 mrad. With 500 nm of liquid, the bright field to dark field transition occurs between 125-175 mrad. Hence, the contrast is now inverted at between 75 mrad and 125 mrad. With 1000 nm of liquid, the contrast is inverted up to 175-200 mrad. If the liquid is thicker than 1500 nm, all ADF contrast below 225 mrad are inverted as bright field images. Therefore, a comparison of the simulated contrast with the images acquired at different collection angles can provide us with an estimate of the liquid layer thickness.

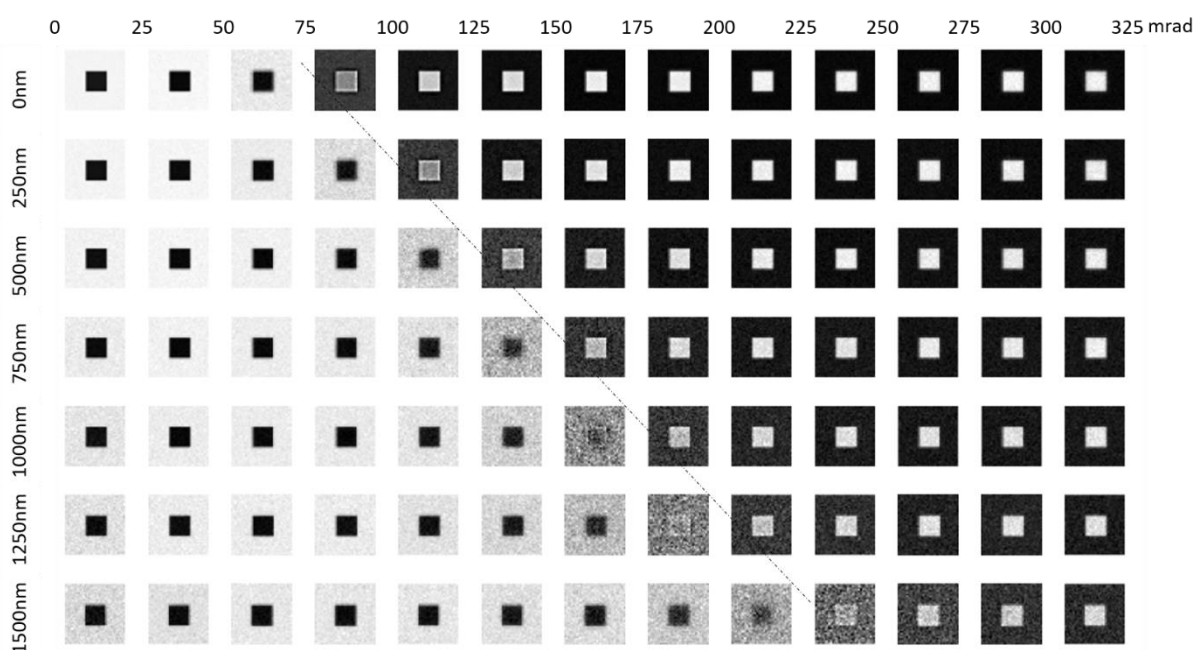


**Figure S5.** The simulated image sequence comparing the contrast over the collection angle and liquid thickness. The angles where the image goes from bright field to dark field occurs are highlighted by the dashed line. On the left hand side of the dashed line are the bright field image where the NP appears darker than the background. On the right hand side of the dashed line are the dark field images where the NP appears brighter than the background.

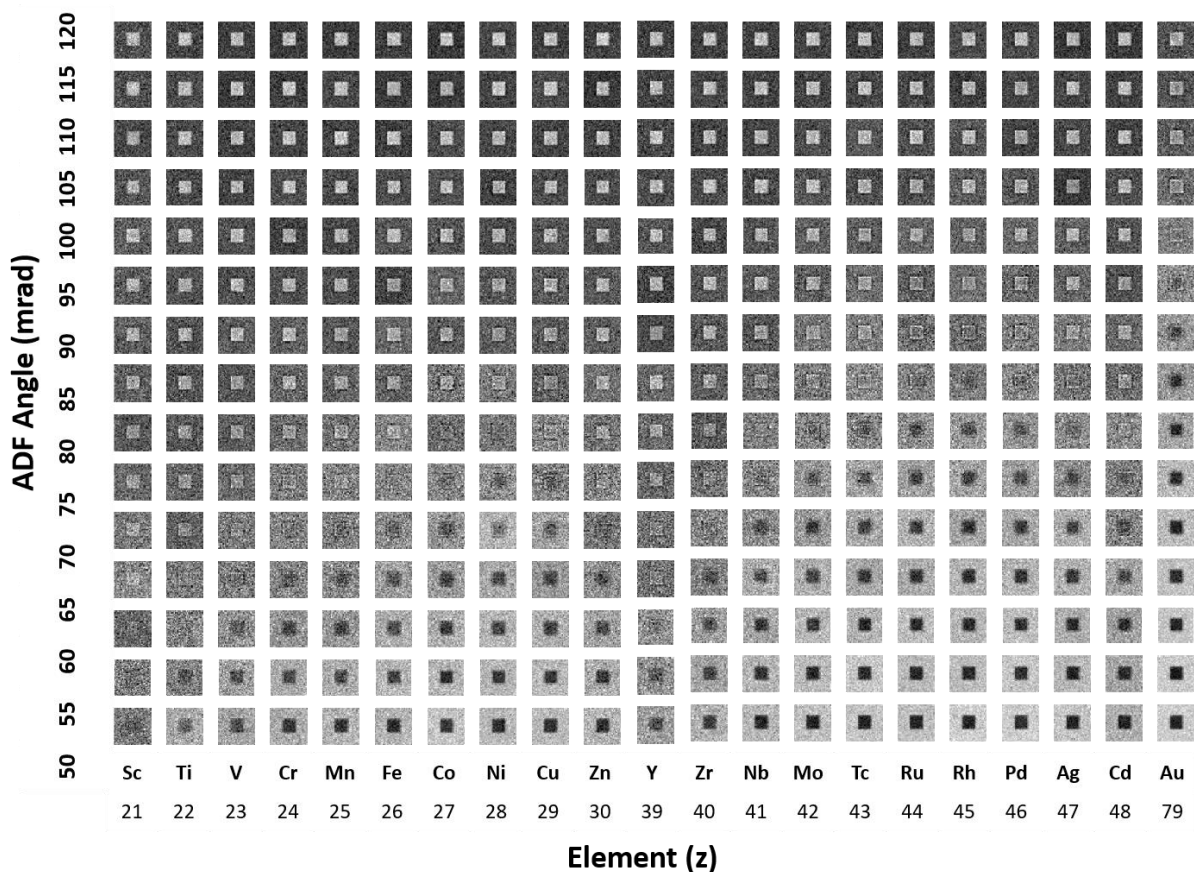


**Figure S6.** The simulated images calculated in the absence of liquid for several transition metal. From Sc to Au, the scattering angle,  $\beta_0$ , where the images switch from BF to DF changes from 55 mrad to 100 mrad. The trend correlates with the atomic scattering factor of the element.

**Table S1: Imaging Conditions and Associated Electron Flux**

	Static image acquisition	Movie recording
Probe current	25 pA	6.3 pA
Dwell time	500 nm	1 $\mu$ s
Nominal resolution (@30 kV, 10 mm WD)	$\sim$ 1 nm	$\sim$ 1 nm
Magnification	$\times$ 150 000	$\times$ 15 000
Pixel size (nm)	$1.8 \times 1.8$	$18 \times 18$ nm
Scan area (pixels)	$1024 \times 884$	$1024 \times 884$
Scan area in $\mu\text{m}^2$	$1.9 \times 1.6 \mu\text{m}^2$	$18.5 \times 16 \mu\text{m}^2$
Electron Flux	$0.53 \text{ e}\cdot\text{\AA}^{-2} \text{ s}^{-1}$	$0.0013 \text{ e}\cdot\text{\AA}^{-2} \text{ s}^{-1}$

## References

Powell, C.J. and Jablonski, A. (2010). NIST Electron Inelastic-Mean-Free-Path Database, Version 1.2, SRD 71. Gaithersburg, MD, National Institute of Standards and Technology.

de Jonge, N., et al. (2009). Electron microscopy of whole cells in liquid with nanometer resolution. *Proceedings of the National Academy of Sciences* 106(7): 2159.

LaVerne, J. A. and S. M. Pimblott (1995). Electron Energy-Loss Distributions in Solid, Dry DNA. *Radiation Research* 141(2): 208-215.

Lin, Y.-H., et al. (2019). In Situ Analysis of Growth Behaviors of Cu<sub>2</sub>O Nanocubes in Liquid Cell Transmission Electron Microscopy. *Analytical Chemistry* 91(15): 9665-9672.